Water-Related Adsorbates on Stepped Platinum Surfaces

Kolb, Manuel Jerome

Chapter 5

Elucidation of Hydrogen TPD Data from High-coverage DFT Calculations

5.1 Abstract

In this work we discuss high-coverage hydrogen adsorption energies and geometries on the stepped platinum surfaces Pt(533) and Pt(553) and link these results with ultra-high-vacuum temperature programmed desorption (TPD) data to elucidate the origin of the desorption features. We find that for the Pt(533) surface hydrogen exhibits two main adsorption energy regimes. The high-temperature peak is linked to the step edge desorption feature, while the low-temperature feature is connected to the terrace desorption. The ratio between the high-temperature and the low-temperature TPD peaks of 1:3 is reproduced by this interpretation and we arrive at a total Pt:H ratio of 1:1 for the Pt(533) surface. For the Pt(553) surface on the other hand, we find that by combining the results from the deconvolution of the experimental desorption traces with our theoretical results that the high-temperature desorption feature is linked to the step edge desorption. By integration of the TPD spec-

trum, we arrive at a 1:2.25 ratio between step desorption and the remaining two peaks. Therefore, we associate these peaks with the two next-most favorable adsorption sites, which are located on the terrace. This suggests a significantly lower 0.6:1 H:Pt ratio for the Pt(553) surface. From our results we conclude that it is possible to elucidate experimental TPD spectra from simulated adsorption energies for the studied surfaces, due to the low desorption barriers present.

Based on: Manuel J. Kolb, Cansin Badan, Anna Garden, Egill Skulason, Ludo B.F. Juurlink, Hannes Jonsson and Marc T.M. Koper, in preparation

5.2 Introduction

Platinum surfaces are an important catalyst for hydrogenation reactions in heterogenous catalysis[1]. In these reactions, the interaction between the catalyst and the adsorbed, dissociated hydrogen plays a key role in the catalytic activity. Furthermore, the adsorption of hydrogen also plays an important role in electrocatalysis[2], where it is linked to the hydrogen evolution reaction. Ultra-high-vacuum techniques can help in gaining insight into the adsorption properties of hydrogen and the influence of defect sites for both these fields. Consequently, multiple experimental studies have focused on the interaction of platinum and hydrogen [3–5]. These studies investigated not only the Pt(111) facet, but also regularly stepped surfaces and the influence of step edges on the adsorption properties of hydrogen. From a theoretical standpoint, multiple studies have dealt with hydrogen adsorption on the Pt(111) surface, and its interaction with co-adsorbates [6, 7], however only limited work was done on surfaces containing defects [8].

A suitable experimental technique to obtain information about interaction and adsorption energies is temperature programmed desorption (TPD). However, in this approach there is not always a clear link between the desorption peak and the microscopic process it stems from. Density functional theory (DFT) calculations can help provide this link and can therefore give a better view of the desorption pathways involved. One successful example of using theoretical calculations to elucidate TPD spectra is hydrogen desorption from the Pt(110)-(2x1)-reconstructed surface [9, 10]. In this study, it was found that varying desorption barriers for different coverages can play a large role in determining the desorption pathways. However, to date no studies were performed on surfaces with lower step densities.

Previous work in our group discussed TPD spectra of deuterium desorbing from the Pt(533) and Pt(553) surfaces [5]. It was found that deuterium exhibits a two peak spectrum on Pt(533), which has a (100) step edge. In contrast, the Pt(553) surface, which has a (111)-type step edge, shows a significantly more complex spectrum. Based on these results, we performed DFT calculations on low-coverage hydrogen adsorption on the Pt(533) and Pt(553) surfaces[11]. We found a very good correlation between the adsorption energies and the desorption spectrum for Pt(533). However, the low-coverage adsorption picture was not adequate for explaining the full hydrogen desorption spectrum on the Pt(553) surface.

In this study we perform simulations of high-coverage hydrogen adsorption on Pt(533) and Pt(553). We find that hydrogen on the step edge of Pt(533) shows a slight attractive interaction, while on Pt(553) this attractive interaction is increased noticeably. Interactions on the terrace are found to be short-ranged and repulsive. Based on these results we identify ranges in the differential Gibbs

adsorption energy distribution for the adsorbates on these surfaces which are directly linked to the desorption peaks. These results help explain why the hydrogen desorption spectra from these two seemingly similar surfaces are so distinctly different.

5.3 Computational Methods

We used the *ab initio* density functional code VASP [12–15] and the PBE functional [16] with PAW projectors [17, 18] for our calculations. The Brillouin zone was sampled using a 3x9x1 grid for the super cell which was chosen to be two atoms wide along the step edge. A plane-wave basis set with a cutoff energy of 550 eV was selected. First-order Methfessel-Paxton smearing [19] with a sigma of 0.2 eV was used and all energies were extrapolated to 0 K. Additional information about the model surfaces can be found in reference [11]. Structures were relaxed until the remaining forces were below 0.04 eV/Å.

The adsorption energies are calculated as Gibbs energies and are corrected for zero-point energy (ZPE) and vibrational entropy at 273 K, following the methods described by Loffreda [20]. The total Gibbs energy for each adsorption structure was calculated as:

$$G_{tot,n\cdot H_{ads}} = E_{DFT,n\cdot H} + ZPE_{n\cdot H} - T \cdot S_{n\cdot H,tot}, \tag{5.1}$$

while the gas-phase references were calculated as

$$G_{tot,\frac{n}{2}\cdot H_2(g)} = E_{DFT,\frac{n}{2}\cdot H_2(g)} + ZPE_{\frac{n}{2}\cdot H_2(g)} - T \cdot S_{\frac{n}{2}\cdot H_{2,tot}(g)}, \tag{5.2}$$

The values for $S_{H_2O,tot}$ are taken from tables for gas-phase species in reference [21]. In order to study the actual energy differences that occur when increasing the coverage, we use the so-called differential (Gibbs) adsorption energies, mirroring previous work on this topic [9, 10]. These are calculated by referencing each energy to the structure with the most favorable energy of all structures with one hydrogen atom less per super cell:

$$G_{diff,n\cdot H_{ads}} = G_{tot,n\cdot H_{ads}} - G_{tot,min,(n-1)\cdot H_{ads}}, \tag{5.3}$$

It should be noted that the ZPE and entropy contributions do not change significantly between different configurations with the same number of adsorbed molecules.

Furthermore, in order to study the influence of barriers on the desorption characteristics of hydrogen from stepped Pt, we performed nudged-elastic-band (NEB) calculations[22]. The barrier calculations were also performed with a cutoff

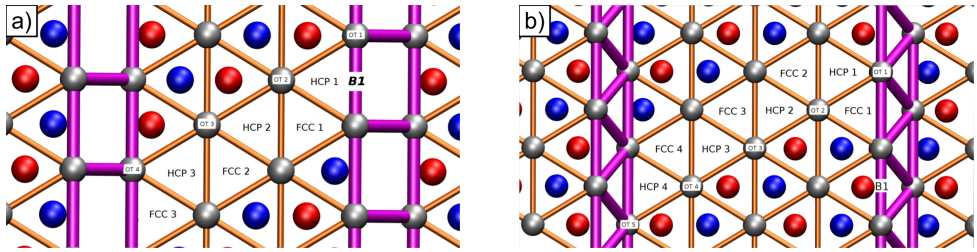

Figure 5.1: Adsorption sites on a) the Pt(533) surface and b) the Pt(553) surface. Surface platinum atoms are marked in silver, first sub-surface layer platinum atoms are represented in blue, while the atoms in the second subsurface layer are shown in red. Figure taken from reference [11]

energy of 550 eV, and were relaxed until the remaining forces orthogonal to the reaction coordinate were below 0.04 eV/Å. The simulations used 7 images along the reaction coordinate. Climbing image NEB calculations [23] for the converged pathways were attempted, but had notable convergence problems even after more than 250 ionic steps. The few calculations that did converge showed no noticeable change in the barrier height compared to the standard NEB calculations.

We use model surfaces for Pt(533) and Pt(553) which are described in more detail in refence [11]. In figure 5.1 we show the naming scheme for the adsorption sites. In this paper the term "coverage" is meant to signify the ratio H:Pt between the number of adsorbed hydrogens per unit cell and the number of surface platinum atoms in the unit cell. We note that it is not always clear what actual H:Pt ratio can be reached under experimental conditions. A clear link to the coverages under experimental conditions will be made in the sections dealing with the elucidation of the TPD spectra. The super cells are identical to the ones in the previous publication [11] and are comprised of two unit cells of the stepped surface replicated along the step edge. This allows for study of isolated hydrogen atoms, as well as for interaction effects at medium to high coverages.

5.4 Results and Discussion

5.4.1 High-Coverage Hydrogen Adsorption on Pt(533) and Desorption Characteristics

In the following we will discuss adsorption structures for increasing coverages of hydrogen on Pt(533). The structures shown are the most favorable configurations for each individual coverage, since we expect that high diffusion rates allow the hydrogen atoms to move to their most favorable positions before the surface

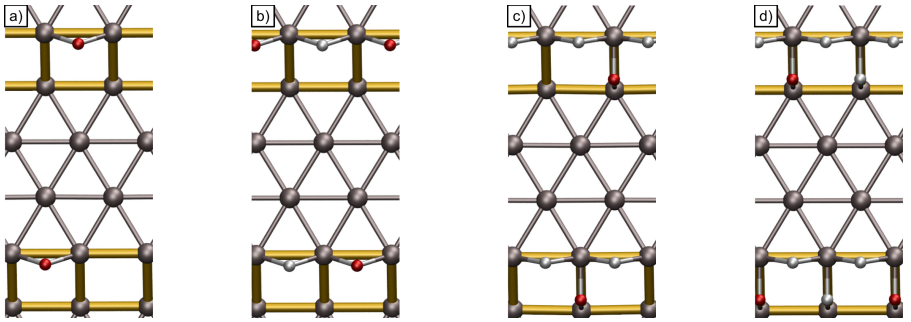

H:Pt 1:8	H:Pt 2:8	H:Pt 3:8	H:Pt 4:8
G_{diff} = -0.56 eV	G_{diff} = -0.59 eV	G_{diff} = -0.36 eV	G_{diff} = -0.36 eV

Figure 5.2: Adsorption structures and their respective differential Gibbs adsorption energies for increasing coverages from a) 1 hydrogen to d) 4 hydrogen atoms per super cell. The atom with the lowest differential Gibbs adsorption energy, which is added to increase the coverage, is marked in red.

reaches the desorption temperature of hydrogen.

1-4 Hydrogen atoms (H:Pt = 1:8 - 4:8): Step-edge related adsorption

The most favorable adsorption site on the Pt(533) surface for a single isolated hydrogen atom is the B1 site at the step edge, as shown in Fig. 5.2a, with a (differential) Gibbs adsorption energy of -0.56 eV [11]. We find that the site favored for the adsorption of the second hydrogen atom in the super cell is the other B1 site at the step edge. The differential Gibbs adsorption energy for this site is -0.59 eV and the resulting adsorption geometry can be seen in Fig. 5.2b. The increase in differential Gibbs adsorption energy indicates that there is a slight attractive interaction of ~ 0.015 eV per atom between hydrogen atoms absorbed at the step edge of Pt(533). Further increasing the coverage to include 3 hydrogen atoms per super cell, we find the most favorable site to be the OT4 site with a differential Gibbs absorption energy of -0.36 eV (see Fig. 5.2c). The OT4 site is located atop the lower step-edge Pt atom but can also be viewed as a bridge site between the upper and lower step-edge platinum atoms. For 4 hydrogen atoms per unit cell we find a preference to occupy the second OT4 site (the resulting adsorption geometry can be found in 5.2d). A differential Gibbs adsorption energy of -0.36 eV was found for this structure. At this point the step edge is completely covered and no further step-related adsorption sides can be occupied without causing strong, unfavorable interactions.

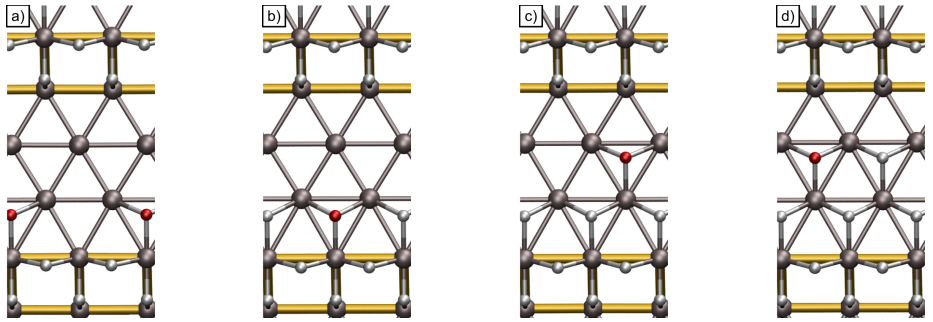

H:Pt 5:8	H:Pt 6:8	H:Pt 7:8	H:Pt 8:8
G_{diff} = -0.32 eV	G_{diff} = -0.32 eV	G_{diff} = -0.31 eV	G_{diff} = -0.31 eV

Figure 5.3: Adsorption structures and their respective differential Gibbs adsorption energies for increasing coverages from a) 5 hydrogen to d) 8 hydrogen atoms per super cell. The atom with the lowest differential Gibbs adsorption energy, which is added to increase the coverage, is marked in red.

5-8 Hydrogen atoms (H:Pt = 5:8 - 8:8): Terrace adsorption

Increasing the coverage beyond 4 hydrogen atoms per super cell leads to the occupation of terrace sites. We find that for 5 hydrogen atoms per super cell, the FCC1 site adjacent to the upper step edge is preferred with a differential Gibbs energy of -0.32 eV. The corresponding adsorption geometry can be seen in Fig. 5.3a. The second terrace-bound atom is found to bind preferentially to the second FCC1 site on the terrace with a differential Gibbs energy of -0.32 eV (see Fig. 5.3b). Increasing the occupation of the super cell further, the two FCC2 sites will be filled next. They exhibibt differential Gibbs energies of -0.31 eV for the first adsorbate and an identical -0.31 eV for the second adsorbate. The resulting adsorption geometries can be seen in figures 5.3c and 5.3d. Note that the differential Gibbs adsorption energy differences between these 4 sites are very small, independent of the exact order of the filling. This observation, combined with the low diffusion barriers, leads us to conclude that there is no fixed order for filling of, or desorbing from, the terrace. A further increase in coverage was not investigated for the following two reasons. Firstly, a surface with 8 hydrogen atoms per super cell is fully covered (H:Pt = 1:1) and there are no low-barrier adsorption pathways available for further adsorption. Additionally, the experimental TPD spectrum shows a 1:3 ratio between high-temperature and low-temperature peak. This ratio is satisfied for the current 1:1 occupation in the DFT simulation, which indicates that no further hydrogen will be adsorbed.

Table 5.1: Additional reaction barriers for the B1-B1 and lowest energy desorption pathways from Pt(533) for increasing coverages.

Ratio H:Pt in super cell	Pathway 1	E_{barr} [eV]	Pathway 2	E_{barr} [eV]
2:8	B1-B1	0.05	—	—
4:8	B1-B1	0.00	OT4-OT4	—*
6:8	B1-B1	0.00	FCC1-FCC1	0.07**
8:8	B1-B1	0.00	FCC2-FCC2	0.08

* Desorption pathway NEB did not converge at given convergence criteria. Pathway barrier energies were consistently above 0.4 eV.

** Calculation did not converge past 0.1 eV/Å remaining forces

5.4.2 Barriers on the Pt(533) Surface

In order to estimate the influence of possible desorption barriers, we performed NEB calculations for the B1-B1 and lowest-energy desorption pathway at each ratio of H:Pt ranging from 1:4 over 2:4 and 3:4 to 4:4. The results are shown in table 5.1. Note that "additional barrier" in this case refers to any energy barrier on top of the desorption energy (adsorption energy) for the two desorbing hydrogen atoms. We find that at all coverages these additional desorption barriers are below 0.1 eV. The only exception is the desorption from the OT4 sites, which exhibits a complicated pathway due to the unique geometry of the surrounding platinum atoms. Unfortunately, none of our attempts to model this pathway led to a successfully converged NEB calculation. All unconverged results showed barriers in excess of 0.4 eV. However, we are certain that this will not play a large role in the actual physical system, since the diffusion barriers from and to the OT4 site are very small. This means that the pathway can proceed via a diffusion step, followed by desorption from the neighboring FCC2 sites.

5.4.3 Elucidation of TPD Spectra

Figure 5.4a) plots the differential Gibbs energies of adsorption as a function of the coverages described above. Additionally, we introduced general energy ranges that contain the adsorption energies of multiple desorption sites. We observe two general regimes of adsorption energies, namely one regime for the highly favorable B1-bound hydrogen (green area in Fig. 5.4) and one regime for the rest of the adsorption sites, which have less favorable adsorption energy (blue area in Fig. 5.4). The step edge related OT4 sites, also fall into the latter regime,

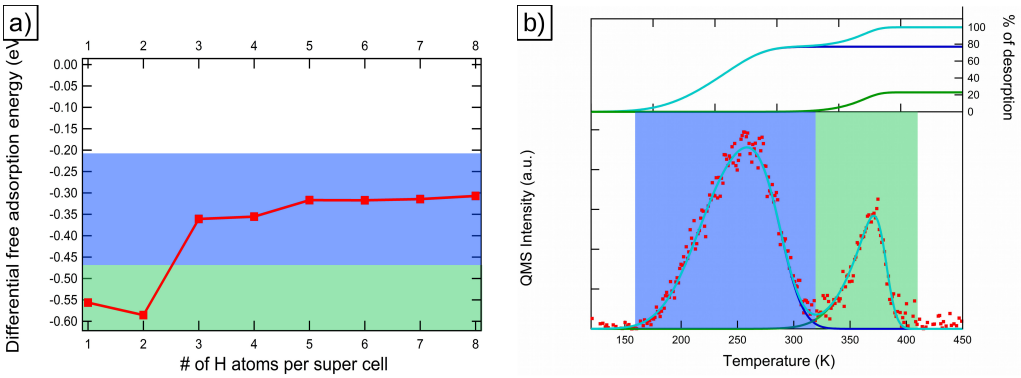

Figure 5.4: a) Differential Gibbs adsorption energies for Pt(533), the two general ranges of adsorption energies discussed below are marked in green (step adsorption) and blue (terrace adsorption), b) TPD spectrum with the colored areas indicating the origin of the peaks in a). Inset in b) shows the integrals of the deconvolution fits (cyan and green) as percentages of the total deconvolution integral (blue)

leading to a 1:3 ratio between the green and the blue areas, which mirrors the experimentally observed ratio of 23:77 or ca. 1:3 [5]. This implies that hydrogen on Pt(533) reaches a ratio of 1H:1Pt and therefore a true 100% coverage. Figure 5.4b) shows the corresponding temperature regions in the experimental TPD spectrum. Furthermore, the attractive interaction between the step-bound hydrogen atoms leads to a slightly sharper peak than the one observed for the terrace, which is reflected in the experimental data.

5.4.4 High-Coverage Hydrogen Adsorption on Pt(553) and Desorption Characteristics

Next we will describe our findings for the Pt(553) surface. We will, as above, only describe the most favorable adsorption geometry for each coverage.

1-2 Hydrogen atoms (H:Pt = 1:10 - 2:10): Step adsorption

In our earlier publication [11], we identified the FCC1 site (see Fig. 5.5a) at the upper step edge with a (differential) Gibbs adsorption energy of -0.24 eV as the most favorable adsorption site for a single hydrogen atom on Pt(553). However, when increasing the occupation to 2 H per super cell, we find that a combination of two B1 sites (see Fig. 5.5b), the same as on Pt(533), is the most favorable adsorption geometry. A differential Gibbs adsorption energy of -0.37 eV

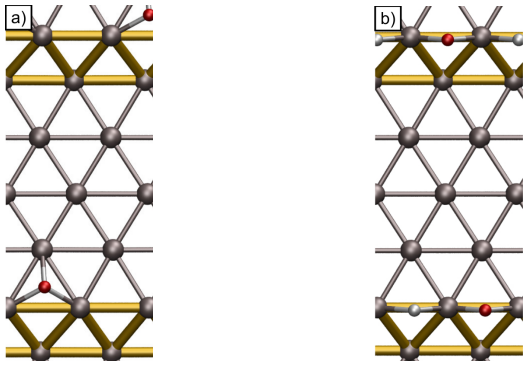

H:Pt 1:10
G_{diff} = -0.24 eV

H:Pt 2:10
G_{diff} = -0.37 eV

Figure 5.5: Adsorption structures and their respective differential Gibbs adsorption energies for increasing occupations from a) 1 hydrogen to b) 2 hydrogen atoms per super cell. The atom with the lowest differential Gibbs adsorption energy, which is added to increase the occupation, is marked in red.

is observed. Note that this indicates a (for hydrogen) strong attractive interaction of $\sim$ 0.07 eV/H. Apparently, this strong interaction should be associated with the change in preferred binding geometry.

2-6 Hydrogen atoms (H:Pt = 3:10 - 6:10): Terrace adsorption

Increasing the occupation beyond 2 hydrogen atoms per super cell, we find that now the FCC3 site (see Fig 5.6a) in the middle of the terrace is the most favorable site with a differential Gibbs adsorption energy of -0.21 eV. The preference of the sites in the middle of the terrace was also visible for the single-adsorbate picture [11]. Increasing the occupation to 4 hydrogen atoms per super cell, the second FCC3 site (see Fig. 5.6b) is occupied. A differential Gibbs energy of -0.20 eV is calculated for this site. Further increasing the occupation to 5 and 6 hydrogen atoms per super cell leads to the filling of the two FCC2 sites on the terrace. The respective differential Gibbs energies of adsorption are -0.15 eV and an identical -0.15 eV. The adsorption geometries can be seen in figures 5.6c and 5.6d. Note that the step-edge adjacent FCC1 sites are not occupied due to the repulsive interaction with the filled B1 sites.

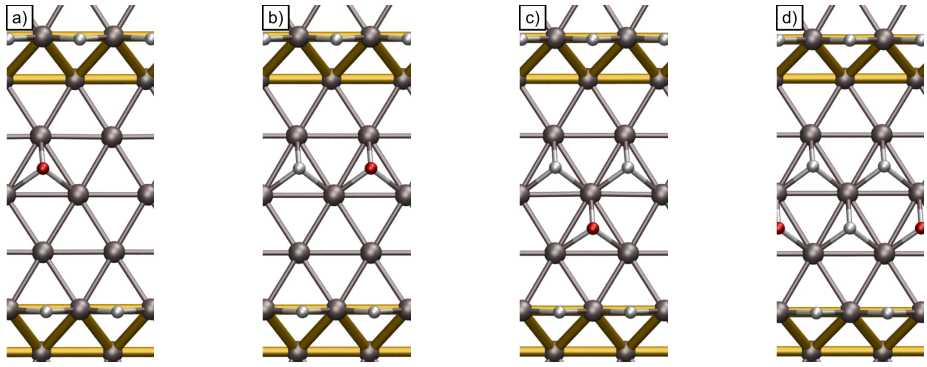

Figure 5.6: Adsorption structures and their respective differential Gibbs adsorption energies for increasing occupations from a) 3 hydrogen to d) 6 hydrogen atoms per super cell. The atom with the lowest differential Gibbs adsorption energy, which is added to increase the occupation, is marked in red.

7-10 Hydrogen atoms: Low Adsorption Energies, Step Adsorption, Complete Restructuring of the Adsorption Geometry

Further increasing the occupation beyond 6 H per cell we observe a drastic decrease in differential Gibbs adsorption energies, to the point that there is little to no energy gain for additional adsorbed H atoms. We will discuss these sites here to arrive at the same 1H:1Pt ratio as for Pt(533), however, we want to point out that it is highly unlikely that these occupations can be reached in the real physical system. This has two main reasons: For any occupation beyond 7 hydrogen atoms per super cell, the adsorption energies are very unfavorable, so adsorption at these sites is energetically possible, but unlikely. Furthermore, for the higher occupations of 9 and 10 hydrogen atoms there are no areas in the unit cell that allow for easy dissociative adsorption of the hydrogen molecule (requiring 2 neighboring, empty FCC sites), leading us to believe that these occupations cannot be reached, at least not in the UHV regime. The first adsorption sites to be filled in this regime are the two weak-binding FCC4 sites at the lower step edge with adsorption energies of -0.05 eV and -0.05 eV, respectively. Their respective adsorption geometries can be seen in figures 5.7a and 5.7b. Increasing the occupation further forces the hydrogen to occupy the OT1 site at the step edge (see Fig. 5.7c), which interacts strongly with the other step-bound hydrogen atoms, especially the B1 site reducing the differential Gibbs adsorption energy to 0.00 eV. Increasing the occupation to 10 H per super cell, we find that shift-

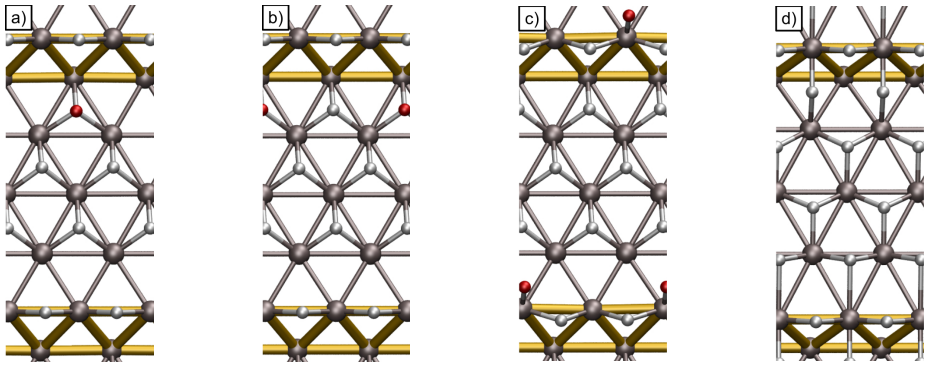

H:Pt 7:10 G_{diff} = -0.05 eV | H:Pt 8:10 G_{diff} = -0.05 eV | H:Pt 9:10 G_{diff} = -0.00 eV | H:Pt 10:10 G_{diff} = -0.05 eV

Figure 5.7: Adsorption structures and their respective differential Gibbs adsorption energies for increasing occupations from a) 7 hydrogen to d) 10 hydrogen atoms per super cell. The atom with the lowest differential Gibbs adsorption energy, which is added to increase the occupation, is marked in red. Geometry d) contains no atom marked in red since the complete geometry shifts to HCP adsorption sites

ing the complete adsorption structure to occupy HCP sites instead of FCC sites leads to a small increase in total adsorption energy compared to the FCC-based 10 H structures. Applying the differential Gibbs adsorption energy methodology, which is somewhat ill-defined in this case, we arrive at a value of -0.04 eV for this adsorption geometry. Please specifically note that the HCP-based geometry for 9 hydrogen atoms per super cell is less favorable than the one containing the OT1-adsorbed hydrogen atom. We find it very unlikely that this adsorption geometry will be present in the real system, due to the size of the combined barrier for the shift from the FCC-based adsorption structure to the HCP-based adsorption structure.

5.4.5 Barriers on the Pt(553) Surface

Also for the Pt(553) surface, NEB barrier calculations were performed, the results of which can be found in table 5.2. As described earlier, “barrier” denotes any additional barrier that needs to be overcome beyond the desorption energy differences. We find that without exception all barriers are below 0.1 eV for all adsorption geometries. The B1-B1 pathway generally shows no additional barrier, while the FCC-FCC desorption usually show very low barriers ranging from 0.03 eV to 0.08 eV. In conclusion this means that also on the Pt(553) surface

Table 5.2: Additional reaction barriers for the B1-B1 and lowest-energy desorption pathways from Pt(553) for increasing occupations.

Ratio H:Pt in super cell	Pathway 1	E_{barr} [eV]	Pathway 2	E_{barr} [eV]
2:10	B1-B1	0.00	—	—
4:10	B1-B1	0.00	FCC3-FCC3	0.03
6:10	B1-B1	0.03	FCC2-FCC2	0.05
8:10 *	B1-B1	0.00	FCC2-FCC2	0.08

* Occupations beyond a ratio of 8:10 were not investigated with NEB calculations. The reasons for this are discussed in the section of the text dealing with these occupations.

desorption barriers play no important role.

5.4.6 Elucidation of TPD Spectra

For the Pt(553) surface, inferring the maximum occupation from the pure DFT data is challenging, since it is uncertain if the occupations of 7-10 hydrogen atoms per super cell are present in the experiment. From our theoretical results we conclude that the most favorable adsorption sites (2 B1 sites) must be linked to the highest-temperature desorption feature. Additionally, we find that the highest temperature TPD peak is sharp compared to all other peaks on the Pt(553) surface, indicating (strong) attractive interactions, which mirrors our findings in DFT (though DFT appears to overestimate the attractive interaction). With the high-temperature peak clearly associated with the step edge, we can now obtain an estimate for the full occupation of the surface by comparing the TPD deconvolution integrals for the low-temperature features to this peak. We find a ratio of 1:2.25 for the ratio between the high-temperature peak and the sum of the integrals of the two low-temperature peaks. This suggests a maximum occupation of 6-7 hydrogen atoms per super cell in our calculations. Furthermore, since the remaining two low-temperature features each show similar total integrals as the high-temperature feature, we can assign these peaks to the two next-best pairs of adsorption sites. Therefore, we deduce that the medium-temperature desorption feature is related to the second and third-best adsorption sites (2 FCC3 sites) and the peak low-temperature desorption peak is related to the fourth and fifth-best sites on the surface (2 FCC2 sites). Figure 5.8a) shows the differential Gibbs adsorption energies for 1-10 hydrogen atoms per super cell, with the three

adsorption energy ranges that were discussed above marked in cyan, black and green. Figure 5.8 shows the TPD spectrum with the deconvolution fits and their integrals. Additionally, the temperature ranges associated with the adsorption sites in a) are marked in the corresponding colors.

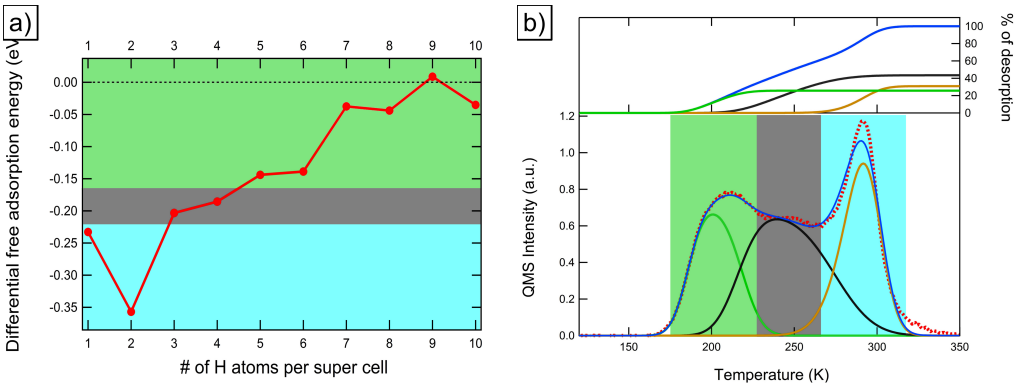

Figure 5.8: a) Differential Gibbs adsorption energies for Pt(553), three general ranges of adsorption energies discussed in the text are marked in cyan (step adsorption), black (terrace adsorption) and blue (low adsorption energy regime), b) TPD spectrum with the colored areas indicating the origin of the peaks in a). Inset in b) shows the integrals of the deconvolution fits (cyan, black and green) as percentages of the total integral (blue)

5.5 Conclusions

From the above DFT results we conclude that the Pt(533) TPD features can be explained by the two main regimes of adsorption energies encountered during the calculations: The high-temperature feature can be linked to the very favorable B1 site at the step edge, while the low-temperature feature can be linked to the 3 occupied terrace sites. The integration of the TPD spectrum supports the observed ratios between step and terrace and suggests a maximum ratio of hydrogen atoms to surface platinum atoms of 1:1. We observe a slight attractive interaction on the step edge of 0.015 eV per hydrogen atom. On the other hand, on the Pt(553) surface we find a more complex adsorption energy landscape. We find that the most favorable adsorption site on the step edge shifts from the FCC1 site, for the lowest occupation studied, to a full occupation of the B1 sites. This is due to a (for hydrogen) remarkably strong attractive interaction of 0.07 eV per hydrogen atom. We combine this knowledge with the integrals obtained from

the deconvolution of the TPD spectra and arrive at a maximum ratio of hydrogen atoms to surface platinum atoms of 0.6:1. This is significantly lower than the value obtained for Pt(533). We assign the two low-temperature features in the TPD to the FCC3 and FCC2 sites, respectively, reproducing the ratio of the integrals of the TPD deconvolution.

5.6 Acknowledgments

We gratefully acknowledge financial support from the Netherlands Organization for Scientific Research (NWO) as a TOP grant awarded to LBFJ and MTMK. This work was sponsored also by the NWO Exacte Wetenschappen, EW (NWO Physical Sciences Division) for the use of supercomputer facilities, with financial support from the Nederlandse Organisatie voor Wetenschappelijk Onderzoek (Netherlands Organisation for Scientific Research, NWO).

5.7 Bibliography

References

(1) Cremer, P. S.; Su, X.; Shen, Y. R.; Somorjai, G. A. *Journal of the American Chemical Society* **1996**, *118*, 2942–2949.

(2) Conway, B.; Tilak, B. *Electrochimica Acta* **2002**, *47*, 3571 –3594.

(3) Christmann, K; Ertl, G; Pignet, T *Surface Science* **1976**, *54*, 365 –392.

(4) Christmann, K.; Ertl, G. *Surface Science* **1976**, *60*, 365 –384.

(5) Van der Niet, M. J. T. C.; den Dunnen, A.; Juurlink, L. B. F.; Koper, M. T. M. *J. Chem. Phys.* **2010**, *132*, 174705.

(6) Norskov, J. K.; Bligaard, T.; Logadottir, A.; Kitchin, J. R.; Chen, J. G.; Pandelov, S.; Stimming, U. *Journal of The Electrochemical Society* **2005**, *152*, J23–J26.

(7) Greeley, J.; Jaramillo, T. F.; Bonde, J.; Chorkendorff, I.; Norskov, J. K. *Nat Mater* **2006**, *5*, 909–913.

(8) Olsen, R.; Badescu, S.; Ying, S.; Baerends, E. *J. Chem. Phys.* **2004**, *120*, 11852–11863.

(9) Gudmundsdóttir, S.; Skúlason, E.; Jónsson, H. *Phys. Rev. Lett.* **2012**, *108*, 156101.

(10) Gudmundsdottir, S.; Skulason, E.; Weststrate, K.-J.; Juurlink, L.; Jonsson, H. *Phys. Chem. Chem. Phys.* **2013**, *15*, 6323–6332.

(11) Kolb, M. J.; Calle-Vallejo, F.; Juurlink, L. B. F.; Koper, M. T. M. *The Journal of Chemical Physics* **2014**, *140* 134708.

(12) Kresse, G.; Hafner, J. *Phys. Rev. B* **1993**, *47*, 558–561.

(13) Kresse, G.; Hafner, J. *Phys. Rev. B* **1994**, *49*, 14251–14269.

(14) Kresse, G.; Furthmller, J. *Computational Materials Science* **1996**, *6*, 15 – 50.

(15) Kresse, G.; Furthmüller, J. *Phys. Rev. B* **1996**, *54*, 11169–11186.

(16) Perdew, J. P.; Burke, K.; Ernzerhof, M. *Phys. Rev. Lett.* **1996**, *77*, 3865–3868.

(17) Blöchl, P. E. *Phys. Rev. B* **1994**, *50*, 17953–17979.

(18) Kresse, G.; Joubert, D. *Phys. Rev. B* **1999**, *59*, 1758–1775.

(19) Methfessel, M.; Paxton, A. T. *Phys. Rev. B* **1989**, *40*, 3616–3621.

(20) Loffreda, D. *Surf. Sci.* **2006**, *600*, 2103 –2112.

(21) Ed. Chase, M.; Davies, C.; Downey, J.; Frurip, D.; MacDonald, R.; Syverud, A., *NIST-JANAF Thermodynamical Tables*, Suppl. 1 to Vol 14 of J. Phys. Chem. Ref. Data, 1985; Vol. 14.

(22) Henkelman, G.; Uberuaga, B. P.; Jnsson, H. *The Journal of Chemical Physics* **2000**, *113*, 9901–9904.

(23) Henkelman, G.; Jónsson, H. *The Journal of Chemical Physics* **2000**, *113*, 9978–9985.